

New method for monitoring voltage stability condition of a bus of an interconnected power system using measurements of the bus variables

D. Hazarika

Electrical Engineering Department, Assam Engineering College, Guwahati-13, Assam, India
 E-mail: dlhazarika@sify.com

Abstract: The study presents a new method for monitoring the voltage stability condition of a bus using measurements of the bus variables. For this purpose, bus real power, bus reactive power and bus voltage of a target/selected bus have to be measured (sampled) for two consecutive time frames. These measured values are used to monitor the voltage stability condition of a bus using the mathematical basis developed in this study. The validity and applicability of the proposed method has been established through simulation on IEEE 30 and IEEE 118 bus system.

Nomenclature

| | |
|--------------------|--|
| N | total number of buses in the system |
| P_i | injected active power at i th bus |
| Q_i | injected reactive power at i th bus |
| $P_i(t)$ | measured value of injected active power at i th bus at time t |
| $Q_i(t)$ | measured value of injected reactive power at i th bus at time t |
| P_{Di} | active power demand at i th bus |
| Q_{Di} | reactive power demand at i bus |
| P_{Gi} | active power generated by i generator |
| Q_{Gi} | reactive power generated by i generator |
| V_i | magnitude of voltage at i bus |
| $V_i(t)$ | measured value of the magnitude of voltage at i th bus at time t |
| δ_i | angle of the bus voltage at i th bus |
| $\cos \phi_i$ | load power factor of the i th load bus |
| $G_{ij} + jB_{ij}$ | element of Y-BUS matrix at i th row and j th column |

1 Introduction

Voltage collapse appears to be a major threat for modern power systems. As a result, voltage stability has become a matter of serious concern for system planners and operators. Voltage stability is threatened when the reactive power demand exceeds the sustainable capacity of the available reactive power of the resources [1]. It has been observed that voltage magnitudes in general, do not give a good

indication of proximity to the voltage stability limit [2]. It is very important that system operators use fast, simple and correct methods to monitor the proximity of voltage collapse of a power system. The voltage collapse index based on a normal load flow solution was proposed to indicate the static voltage stability condition of a power system [3–9]. Continuation power flow analysis is based on a locally parametrised continuation technique. It aims at avoiding the singularity of the Jacobian by slightly reformulating the power flow equations [10]. A network partitioning technique has been employed for investigating the voltage stability condition of a load bus [11]. Most of the methods are based on executing a large number of power flows using conventional models.

Realising that the network phasor measurement contains enough information for monitoring voltage stability at a local load supply node, researchers have developed several algorithms that use voltage and current phasor measurements to monitor system voltage stability. The on-line monitoring of voltage instability of a power system based on the phasor measurement unit (PMU) local measurements has drawn wide attention [12–19] in the field of power system research. A PMU is a device which measures the electrical waves on an electricity grid, using a common time source for synchronisation. Time synchronisation allows for synchronised real-time measurement of multiple remote measurement points on the grid. Vu *et al.* [12] proposed a stability index that uses the local voltage and current phasor measurements of a load bus. It uses the continuous voltage and current phasor measurements of a load bus to calculate the Thevenin equivalent parameters of the system with respect to a load bus. A simple, computationally very fast local voltage-stability index (VSI) has been proposed using Tellegen's theorem [14], which is based on two consecutive

measurements of a bus. Therefore local phasor measurement unit (PMU) is required to implement this method. A VSI called equivalent node voltage collapse index has been proposed [16], which is based on the ‘equivalent system model’ (ESM) of a load bus of a power system. The ESM is represented using the effect of the system buses on the load bus under consideration. An equivalent local network model (ELNM) has been used for this purpose. The ELNM requires the parameters of the transmission lines connected to the load bus and voltage phasors of the system buses that are connected to the load bus. Therefore PMUs are required in all connecting buses and at the selected bus to implement the method.

A line-based VSI fast-voltage stability index (FVSI) has been proposed [20], the criteria adopted in the paper was to set the discriminant of the root of the receiving end voltage of a transmission line greater than zero (i.e. non-existence of solution for receiving end voltage). The measurements required for the calculation of FVSI are – (i) the reactive power flow at the receiving end and (ii) voltage magnitude at sending end of the transmission line along with the parameters of the transmission line. However, this index and method do not have a strong and strict theoretical basis [21].

Owing to transformer on-load-tap changers dynamics, the incoming voltage instability increases its speed. Therefore a short-time frame interval of PMU measurements and high-speed computing facilities are required to track the voltage instability condition of a power system in real time. A scheme is proposed to monitor the voltage stability condition with change in transformer tap setting [22] using PMU measurements. Time synchronised measurements of voltage and current before and after a tap position change are used to compute a VSI in real time. To simulate the environment for real-time operation and monitoring of the voltage stability condition with a change in transformer tap setting, two workstations with dual-Xeon processor of 3.2 GHz were used as a real-time station (RTS) and a real-time monitoring station (RMS). The analogue link between RTS and RMS consists of two field programmable gate arrays (FPGAs) I/O cards. It simulates the data link between the PMU and the system control centre. The FPGA cards also control two sets of 16 bit D/A and A/D converter having a sampling rate of 100 MHz. The scheme is simple and fast enough to implement in a real-time application. The time interval between two consecutive measurements of bus variables is proposed as 500 ms for real-time monitoring of the voltage stability condition of a power system [23].

In this paper, a new method is proposed for monitoring the voltage stability of a power system based on two consecutive measurements of the variables of a bus. For this purpose, bus real power, bus reactive power and bus voltage of a target/selected bus have to be measured for two consecutive time frames. Using these measurements, the elements of the Jacobian matrix of the two bus equivalent system (TBES) with respect to the target bus are determined. The determinant of the Jacobian matrix of this TBES indicates the voltage stability condition of the system. The system voltage collapse occurs, when it becomes zero. A sensitivity relation between the change in the determinant of the Jacobian matrix of the TBES with respect to change in real-power injection at the target bus has been developed using the elements of the Jacobian matrix of the TBES and its bus voltage magnitude. This relation is then used to predict the critical load of the bus with respect to its voltage stability limit.

2 Problem formulation

A TBES of an interconnected power system with an equivalent source and a target bus k can be represented as shown in Fig. 1.

Where G_{kk} , B_{kk} , G_{kG} and B_{kG} are the elements of the bus admittance matrix $[Y]$ for the TBES. $V_G \angle \delta_G$ represents the equivalent voltage of the TBES with respect to target bus k . It is to be noted that G_{kk} , B_{kk} , G_{kG} , B_{kG} , V_G and δ_G are implicit functions of the system states. Therefore they would keep changing depending on the operating state of the system. P_k , Q_k , V_k and δ_k are the bus variables of the target bus k .

The real and reactive power injections at the target k th bus of the TBES can be expressed as

$$P_k = G_{kk}V_k^2 + V_GV_k(G_{kG} \cos(\delta_{kG}) + B_{kG} \sin(\delta_{kG})) \quad (1)$$

$$Q_k = -B_{kk}V_k^2 + V_GV_k(G_{kG} \sin(\delta_{kG}) - B_{kG} \cos(\delta_{kG})) \quad (2)$$

The load flow Jacobian for the TBES can be expressed as

$$\begin{bmatrix} \Delta P_k \\ \Delta Q_k \end{bmatrix} = \begin{bmatrix} \frac{\partial P_k}{\partial \delta_k} & \frac{\partial P_k}{\partial V_k} \\ \frac{\partial Q_k}{\partial \delta_k} & \frac{\partial Q_k}{\partial V_k} \end{bmatrix} \begin{bmatrix} \Delta \delta_k \\ \Delta V_k \end{bmatrix} \quad (3)$$

The elements of the Jacobian matrix for the TBES can be expressed as

$$\frac{\partial P_k}{\partial \delta_k} = V_GV_k(-G_{kG} \sin(\delta_{kG}) + B_{kG} \cos(\delta_{kG})) \quad (4)$$

$$\frac{\partial P_k}{\partial V_k} = 2G_{kk}V_k + V_G(G_{kG} \cos(\delta_{kG}) + B_{kG} \sin(\delta_{kG})) \quad (5)$$

$$\frac{\partial Q_k}{\partial \delta_k} = V_GV_k(G_{kG} \cos(\delta_{kG}) + B_{kG} \sin(\delta_{kG})) \quad (6)$$

$$\frac{\partial Q_k}{\partial V_k} = -2B_{kk}V_k + V_G(G_{kG} \sin(\delta_{kG}) - B_{kG} \cos(\delta_{kG})) \quad (7)$$

Applying (1) and (2) in (4)–(7), the element of the Jacobian matrix of the TBES can be expressed as

$$\frac{\partial P_k}{\partial \delta_k} = -Q_k - B_{kk}V_k^2 \quad (8)$$

$$\frac{\partial P_k}{\partial V_k} = \frac{P_k}{V_k} + G_{kk}V_k \quad (9)$$

$$\frac{\partial Q_k}{\partial \delta_k} = P_k - G_{kk}V_k^2 \quad (10)$$

$$\frac{\partial Q_k}{\partial V_k} = \frac{Q_k}{V_k} - B_{kk}V_k \quad (11)$$

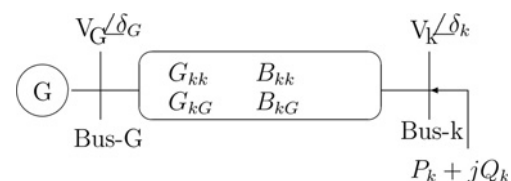


Fig. 1 Equivalent two bus system with target k th bus, Y -bus elements and an equivalent source

Equations (9) and (11) are rearranged to represent G_{kk} and B_{kk} in terms of the element of the Jacobian matrix of the TBES, bus injections and bus voltage of k th bus.

$$G_{kk} = \frac{1}{V_k} \left[\frac{\partial P_k}{\partial V_k} - \frac{P_k}{V_k} \right] \quad (12)$$

$$B_{kk} = \frac{1}{V_k} \left[\frac{Q_k}{V_k} - \frac{\partial Q_k}{\partial V_k} \right] \quad (13)$$

3 Representation of elements of the Jacobian matrix for the TBES using the measurements of the bus variables

Using the bus measurement variables of the k th bus for two consecutive time samples t_1 and t_2 and taking t_2 as reference time, we can represent $(\partial P_k/\partial V_k)$ and $(\partial Q_k/\partial V_k)$ as follows

$$\frac{\Delta P_k}{\Delta V_k} = \frac{\partial P_k}{\partial V_k} = \frac{P_k(t_2) - P_k(t_1)}{V_k(t_2) - V_k(t_1)} \quad (14)$$

$$\frac{\Delta Q_k}{\Delta V_k} = \frac{\partial Q_k}{\partial V_k} = \frac{Q_k(t_2) - Q_k(t_1)}{V_k(t_2) - V_k(t_1)} \quad (15)$$

Therefore (12) and (13) can be expressed with the measured variables as follows

$$G_{kk} = \frac{1}{V_k(t_2)} \left[\frac{\Delta P_k}{\Delta V_k} - \frac{P_k(t_2)}{V_k(t_2)} \right] \quad (16)$$

$$B_{kk} = \frac{1}{V_k(t_2)} \left[\frac{Q_k(t_2)}{V_k(t_2)} - \frac{\Delta Q_k}{\Delta V_k} \right] \quad (17)$$

Now, it is possible to express $(\Delta P_k/\Delta \delta_k)$ and $(\Delta Q_k/\Delta \delta_k)$ with measured variables as follows

$$\begin{aligned} \frac{\Delta P_k}{\Delta \delta_k} &= \frac{\partial P_k}{\partial \delta_k} = -Q_k(t_2) - B_{kk} V_k^2(t_2) \\ &= -Q_k(t_2) - \frac{1}{V_k(t_2)} \left[\frac{Q_k(t_2)}{V_k(t_2)} - \frac{\Delta Q_k}{\Delta V_k} \right] V_k^2(t_2) \\ &= -2Q_k(t_2) + V_k(t_2) \frac{\Delta Q_k}{\Delta V_k} \end{aligned} \quad (18)$$

$$\begin{aligned} \frac{\Delta Q_k}{\Delta \delta_k} &= \frac{\partial Q_k}{\partial \delta_k} = P_k(t_2) - G_{kk} V_k^2(t_2) \\ &= P_k(t_2) - \frac{1}{V_k(t_2)} \left[\frac{\Delta P_k}{\Delta V_k} - \frac{P_k(t_2)}{V_k(t_2)} \right] V_k^2(t_2) \\ &= 2P_k(t_2) - V_k(t_2) \frac{\Delta P_k}{\Delta V_k} \end{aligned} \quad (19)$$

Equations (14), (15), (18) and (19) represent the elements of the Jacobian matrix of the TBES.

At the point of voltage collapse, the determinant of the Jacobian matrix will become zero, that is

$$\text{Det}|J| = J_{Dt} = \frac{\partial P_k}{\partial \delta_k} \frac{\partial Q_k}{\partial V_k} - \frac{\partial P_k}{\partial V_k} \frac{\partial Q_k}{\partial \delta_k} \quad (20)$$

$$= \frac{\Delta P_k}{\Delta \delta_k} \frac{\Delta Q_k}{\Delta V_k} - \frac{\Delta P_k}{\Delta V_k} \frac{\Delta Q_k}{\Delta \delta_k} = 0 \quad (21)$$

The determinant of the Jacobian matrix of the TBES would indicate the voltage stability condition of the bus and that of the system as a whole. At the proximity of voltage collapse it becomes zero.

4 Sensitivity relation between change in real-power injection (ΔP_k) and change in determinant of the Jacobian matrix (ΔJ_{Dt}) of the TBES

The change in determinant value of the Jacobian matrix of the TBES with respect to change in V_k and δ_k can be expressed as

$$\Delta J_{Dt} = \frac{\partial J_{Dt}}{\partial \delta_k} \Delta \delta_k + \frac{\partial J_{Dt}}{\partial V_k} \Delta V_k = \left[\frac{\partial J_{Dt}}{\partial \delta_k} \quad \frac{\partial J_{Dt}}{\partial V_k} \right] \begin{bmatrix} \Delta \delta_k \\ \Delta V_k \end{bmatrix} \quad (22)$$

The term, $(\partial J_{Dt}/\partial \delta_k)$ can be expressed as

$$\begin{aligned} \frac{\partial J_{Dt}}{\partial \delta_k} &= \left[\frac{\partial P_k}{\partial \delta_k} \frac{\partial(\partial Q_k/\partial V_k)}{\partial \delta_k} + \frac{\partial Q_k}{\partial V_k} \frac{\partial(\partial P_k/\partial \delta_k)}{\partial \delta_k} \right] \\ &\quad - \left[\frac{\partial P_k}{\partial V_k} \frac{\partial(\partial Q_k/\partial \delta_k)}{\partial \delta_k} + \frac{\partial Q_k}{\partial \delta_k} \frac{\partial(\partial P_k/\partial V_k)}{\partial \delta_k} \right] \end{aligned} \quad (23)$$

The terms

$$\begin{aligned} \frac{\partial(\partial Q_k/\partial V_k)}{\partial \delta_k}, \quad \frac{\partial(\partial P_k/\partial \delta_k)}{\partial \delta_k}, \quad \frac{\partial(\partial Q_k/\partial \delta_k)}{\partial \delta_k} \quad \text{and} \\ \frac{\partial(\partial P_k/\partial V_k)}{\partial \delta_k} \end{aligned}$$

are derived utilising equations from (4) to (7). It is ensured that they contain only the element of the Jacobian matrix of the TBES and the bus voltage of the target bus since they are already determined by using the measurements of bus variables.

$$\begin{aligned} \frac{\partial(\partial Q_k/\partial V_k)}{\partial \delta_k} &= V_G (G_{kG} \cos(\delta_{kG}) + B_{kG} \sin(\delta_{kG})) \\ &= \frac{(\partial Q_k/\partial \delta_k)}{V_k} = \frac{(\Delta Q_k/\Delta \delta_k)}{V_k(t)} \end{aligned} \quad (24)$$

$$\begin{aligned} \frac{\partial(\partial P_k/\partial \delta_k)}{\partial \delta_k} &= -V_G V_k (G_{kG} \cos(\delta_{kG}) + B_{kG} \sin(\delta_{kG})) \\ &= -\frac{\partial Q_k}{\partial \delta_k} = -\frac{\Delta Q_k}{\Delta \delta_k} \end{aligned} \quad (25)$$

$$\begin{aligned} \frac{\partial(\partial Q_k/\partial \delta_k)}{\partial \delta_k} &= V_G V_k (-G_{kG} \sin(\delta_{kG}) + B_{kG} \cos(\delta_{kG})) \\ &= \frac{\partial P_k}{\partial \delta_k} = \frac{\Delta P_k}{\Delta \delta_k} \end{aligned} \quad (26)$$

$$\begin{aligned} \frac{\partial(\partial P_k/\partial V_k)}{\partial \delta_k} &= V_G (-G_{kG} \sin(\delta_{kG}) + B_{kG} \cos(\delta_{kG})) \\ &= \frac{(\partial P_k/\partial \delta_k)}{V_k} = \frac{(\Delta P_k/\Delta \delta_k)}{V_k(t)} \end{aligned} \quad (27)$$

Substituting

$$\frac{\partial(\partial Q_k/\partial V_k)}{\partial \delta_k}, \quad \frac{\partial(\partial P_k/\partial \delta_k)}{\partial \delta_k}, \quad \frac{\partial(\partial Q_k/\partial \delta_k)}{\partial \delta_k} \quad \text{and} \quad \frac{\partial(\partial P_k/\partial V_k)}{\partial \delta_k}$$

of (24)–(27) in (23) we have

$$\begin{aligned} \frac{\partial J_{Dt}}{\partial \delta_k} &= \frac{\Delta Q_k}{\Delta \delta_k} \left[\frac{1}{V_k(t)} \frac{\Delta P_k}{\Delta \delta_k} - \frac{\Delta Q_k}{\Delta V_k} \right] \\ &\quad - \frac{\Delta P_k}{\Delta \delta_k} \left[\frac{1}{V_k(t)} \frac{\Delta Q_k}{\Delta \delta_k} + \frac{\Delta P_k}{\Delta V_k} \right] \end{aligned} \quad (28)$$

Similarly, the term $(\partial J_{Dt}/\partial V_k)$ can be expressed as

$$\begin{aligned} \frac{\partial J_{Dt}}{\partial V_k} &= \left[\frac{\partial P_k}{\partial \delta_k} \frac{\partial(\partial Q_k/\partial V_k)}{\partial V_k} + \frac{\partial Q_k}{\partial V_k} \frac{\partial(\partial P_k/\partial \delta_k)}{\partial V_k} \right] \\ &\quad - \left[\frac{\partial P_k}{\partial V_k} \frac{\partial(\partial Q_k/\partial \delta_k)}{\partial V_k} + \frac{\partial Q_k}{\partial \delta_k} \frac{\partial(\partial P_k/\partial V_k)}{\partial V_k} \right] \end{aligned} \quad (29)$$

Utilising equations from (4) to (7), we have

$$\frac{\partial(\partial Q_k/\partial V_k)}{\partial V_k} = -2B_{kk} = -\frac{2}{V_k(t)} \left[\frac{Q_k(t)}{V_k(t)} - \frac{\Delta Q_k}{\Delta V_k} \right] \quad (30)$$

$$\begin{aligned} \frac{\partial(\partial P_k/\partial \delta_k)}{\partial V_k} &= V_G(-G_{kG} \sin(\delta_{kG}) + B_{kG} \cos(\delta_{kG})) \\ &= \frac{(\partial P_k/\partial \delta_k)}{V_k} = \frac{(\Delta P_k/\Delta \delta_k)}{V_k(t)} \end{aligned} \quad (31)$$

$$\begin{aligned} \frac{\partial(\partial Q_k/\partial \delta_k)}{\partial V_k} &= V_G(G_{kG} \cos(\delta_{kG}) + B_{kG} \sin(\delta_{kG})) \\ &= \frac{(\partial Q_k/\partial \delta_k)}{V_k} = \frac{(\Delta Q_k/\Delta \delta_k)}{V_k(t)} \end{aligned} \quad (32)$$

$$\frac{\partial(\partial P_k/\partial V_k)}{\partial V_k} = 2G_{kk} = \frac{2}{V_k(t)} \left[\frac{\Delta P_k}{\Delta V_k} - \frac{P_k(t)}{V_k(t)} \right] \quad (33)$$

Substituting

$$\frac{\partial(\partial Q_k/\partial V_k)}{\partial V_k}, \quad \frac{\partial(\partial P_k/\partial \delta_k)}{\partial V_k}, \quad \frac{\partial(\partial Q_k/\partial \delta_k)}{\partial V_k} \quad \text{and} \quad \frac{\partial(\partial P_k/\partial V_k)}{\partial V_k}$$

of (30)–(33) in (29) we have

$$\begin{aligned} \frac{\partial J_{Dt}}{\partial V_k} &= \frac{\Delta P_k}{\Delta \delta_k} \left[-\frac{2}{V_k(t)} \left[\frac{Q_k(t)}{V_k} - \frac{\Delta Q_k}{\Delta V_k} \right] + \frac{1}{V_k(t)} \frac{\Delta Q_k}{\Delta V_k} \right] \\ &\quad - \frac{\Delta Q_k}{\Delta \delta_k} \left[\frac{1}{V_k(t)} \frac{\Delta P_k}{\Delta V_k} + \frac{2}{V_k(t)} \left[\frac{\Delta P_k}{\Delta V_k} - \frac{P_k(t)}{V_k(t)} \right] \right] \end{aligned} \quad (34)$$

To relate change in the determinant of the Jacobian matrix of the TBES to the change in real-power injection at target bus k , variables $\Delta \delta_k$ and ΔV_k of (22) are replaced by ΔP_k and ΔQ_k as

follows

$$\begin{aligned} \Delta J_{Dt} &= \begin{bmatrix} \frac{\partial J_{Dt}}{\partial \delta_k} & \frac{\partial J_{Dt}}{\partial V_k} \end{bmatrix} \begin{bmatrix} \frac{\partial P_k}{\partial \delta_k} & \frac{\partial P_k}{\partial V_k} \\ \frac{\partial Q_k}{\partial \delta_k} & \frac{\partial Q_k}{\partial V_k} \end{bmatrix}^{-1} \begin{bmatrix} \Delta P_k(t_2) \\ \Delta Q_k(t_2) \end{bmatrix} \\ &= \begin{bmatrix} \frac{\partial J_{Dt}}{\partial \delta_k} & \frac{\partial J_{Dt}}{\partial V_k} \end{bmatrix} \begin{bmatrix} \frac{\Delta P_k}{\Delta \delta_k} & \frac{\Delta P_k}{\Delta V_k} \\ \frac{\Delta Q_k}{\Delta \delta_k} & \frac{\Delta Q_k}{\Delta V_k} \end{bmatrix}^{-1} \begin{bmatrix} \Delta P_k(t_2) \\ \Delta Q_k(t_2) \end{bmatrix} \\ &= f_t' \Delta P_k(t_2) + f_t'' \Delta Q_k(t_2) \\ &= f_t' \Delta P_k(t_2) + f_t'' \tan \phi_k \Delta P_k(t_2); \text{ for same load } pf \\ &= (f_t' + f_t'' \tan \phi_k) \Delta P_k(t_2) = f_t \Delta P_k(t_2) \end{aligned} \quad (35)$$

The sensitivity factor f_t increases as the proximity of voltage collapse is approached. Therefore a higher value of f_t would also indicate the proximity of voltage collapse.

5 Prediction of load margin of the k th bus

The Jacobian matrix of the TBES reduces with increase in load at the target bus and it becomes zero at the point of voltage collapse (VCP). The required change in J_{Dt} with respect to the VCP for a bus can be expressed as

$$\Delta J_{Dt}^{VCP} = J_{Dt}^{VCP} - J_{Dt} = 0 - J_{Dt} = -J_{Dt} \quad (36)$$

The corresponding change in bus injection for the k th bus with respect to its VCP can be expressed as

$$\Delta P_{kt}^{VCP} = \frac{-J_{Dt}}{f_t} \quad (37)$$

Therefore load margin of the k th bus with respect to the VCP can be expressed as

$$\Delta P_{Dkt}^{\text{margin}} = -\Delta P_{kt} = \frac{J_{Dt}}{f_t} \quad (38)$$

Now, predicted critical load for k th load bus with respect to its VCP is

$$P_{Dkt}^{\text{predt}} = P_{Dkt} + \Delta P_{Dkt}^{\text{margin}} \quad (39)$$

$\Delta P_{Dkt}^{\text{margin}}$ is determined using the elements of the Jacobian matrix of the TBES. As, G_{kk} , B_{kk} , G_{kG} , B_{kG} , V_G and δ_G are implicit functions of the system states (for a power system these are non-linear), therefore the relation between ΔJ_{Dt} and ΔP_k represented by (35) would also be implicit and be non-linear functions of the system states. Therefore the load margin represented by (38) would be considerably high, if the bus is far from the proximity of voltage collapse. Hence, it is required to normalise the predicted load (P_{Dkt}^{predt}), so that it remains within the actual critical load of the bus with respect to its voltage collapse point. It is observed that the change of J_{Dt} is non-linear with respect to the change in load for the target bus. Therefore the critical load value for the k th load bus is represented by normalising predicted

load (P_{Dkt}^{predt}) as follows

$$P_{Dkt}^{crt} = \frac{P_{Dkt}^{predt}}{1 + \log_{10} [(P_{Dkt}^{predt})/P_{Dkt}]^n} \quad (40)$$

P_{Dkt}^{predt} will be higher, when the bus is far from the proximity of voltage collapse. Therefore the term $[(P_{Dkt}^{predt})/P_{Dkt}]$ will be higher and $1 + \log_{10} [(P_{Dkt}^{predt})/P_{Dkt}]^n$ will be greater than 1 and P_{Dkt}^{crt} will be less than P_{Dkt}^{predt} . As the system approaches the proximity of voltage collapse the term $[(P_{Dkt}^{predt})/P_{Dkt}]^n$ becomes 1 and the $\log_{10} [(P_{Dkt}^{predt})/P_{Dkt}]^n$ becomes 0. The term n is used to adjust the normalisation effect to ensure that the predicted critical load P_{Dkt}^{crt} remains below the actual load at which system collapse would take place.

6 Procedure for the implementation of the method

Implementation of the proposed method requires the measurement of bus real power, bus reactive power and bus voltage of a target bus for two consecutive time frames. These measurements may be captured either from a digital power meter [having arrangement for sampling – (i) real power P , (ii) reactive power Q and (iii) voltage V] or they may be extracted from the measurements of a local PMU. It shows that it is required to move along the negative slope of the $J_{Dt} - P_{Dk}$ curve to determine the critical load of a bus with respect to its VCP. Therefore the time references for two consecutive bus measurements are to be arranged in such a way that $P_{Dk}(t_2) > P_{Dk}(t_1)$ to make the normalisation of predicted load effective (both for increase in load or decrease in load). The procedure for the implementation of the proposed method is provided in the steps given below:-

1. Measure $P_k(t_1)$, $Q_k(t_1)$, $V_k(t_1)$, $P_k(t_2)$, $Q_k(t_2)$ and $V_k(t_2)$ for the selected k th bus for two consecutive time references t_1 and t_2 .
2. Use (14) and (15) to determine $(\Delta P_k/\Delta V_k)$ and $(\Delta Q_k/\Delta V_k)$.
3. Use (18) and (19) to determine $(\Delta P_k/\Delta \delta_k)$ and $(\Delta Q_k/\Delta \delta_k)$.
4. Determine J_{Dt} using (21).
5. Determine $(\partial J_{Dt}/\partial \delta_k)$ and $(\partial J_{Dt}/\partial V_k)$ using (28) and (34), respectively. Finally, determine f_t using (35).
6. Use (39) and (40) to determine P_{Dkt}^{predt} and P_{Dkt}^{crt} , respectively.

7 Simulation results and discussions

To verify the validity and applicability of the proposed method, simulations were carried out on IEEE 30 bus and IEEE 118 bus systems. The aim of the simulations was to examine the nature of change of J_{Dt} at different load buses of IEEE 30 and IEEE 118 bus system with respect to change in load at these buses. For this purpose, load at a target bus is increased using a continuation load flow analysis, where the increment of load is carried out till the load flow analysis tends to arrive at the state of non-convergence to indicate the proximity of voltage collapse of the system. Two consecutive load increment steps of the continuation load flow analysis are taken as the time references t_1 and t_2 , respectively, and accordingly $P_k(t_1)$, $Q_k(t_1)$, $V_k(t_1)$, $P_k(t_2)$, $Q_k(t_2)$ and $V_k(t_2)$ are assigned from the two consecutive load flow analyses to determine – (i) determinant J_{Dt} , (ii) sensitivity factor f_t , (iii) P_{Dkt}^{predt} and

(iv) normalising predicted load P_{Dkt}^{crt} of the target bus with $n = 1$ and $n = 1.5$.

Figs. 2–4 illustrate the variation of J_{Dt} values for the buses 29, 21 and 7 of the IEEE 30 bus system with respect to change in load (P_{Dk}) at 29, 21 and 7 individually. Figs. 5–7 illustrate the variation of J_{Dt} values for the buses 118, 88 and 45 of the IEEE 118 bus system with respect to change in load (P_{Dk}) at 118, 88 and 45 individually.

It has been observed that variation of J_{Dt} is non-linear and reduces sharply with increase in load near the proximity of voltage collapse. Finally, at the VCP it becomes zero. It is observed that the J_{Dt} value of the TBES for IEEE 30 and 118 bus systems has different initial values for different target buses. Therefore it may be concluded that the J_{Dt}

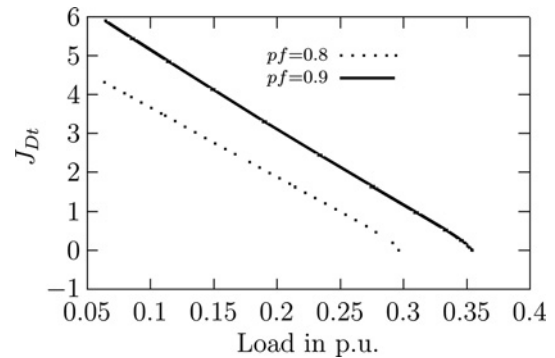


Fig. 2 $J_{Dt} - P_{Dk}$ curve for bus number 29 bus of IEEE 30 bus system, with load power factors $pf = 0.8$ and $pf = 0.9$

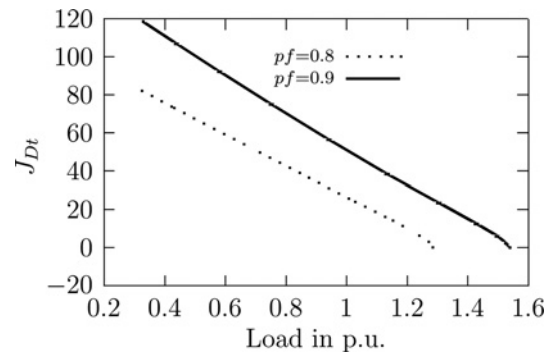


Fig. 3 $J_{Dt} - P_{Dk}$ curve for bus number 21 bus of IEEE 30 bus system, with load power factors $pf = 0.8$ and $pf = 0.9$

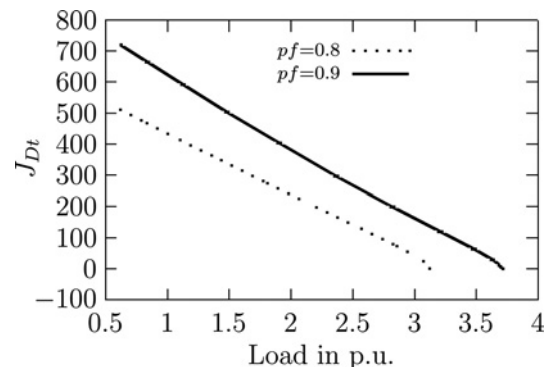


Fig. 4 $J_{Dt} - P_{Dk}$ curve for bus number 7 bus of IEEE 30 bus system, with load power factors $pf = 0.8$ and $pf = 0.9$

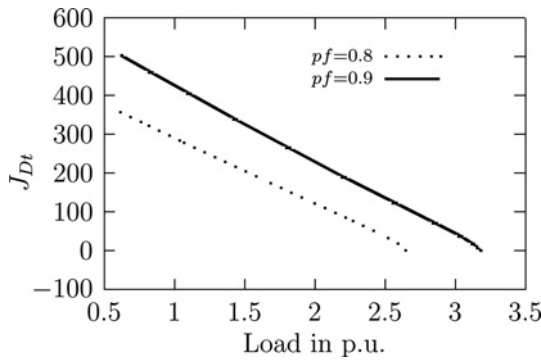


Fig. 5 $J_{Dt} - P_{Dk}$ curve for bus number 118 bus of IEEE 118 bus system, with load power factors $pf = 0.8$ and $pf = 0.9$

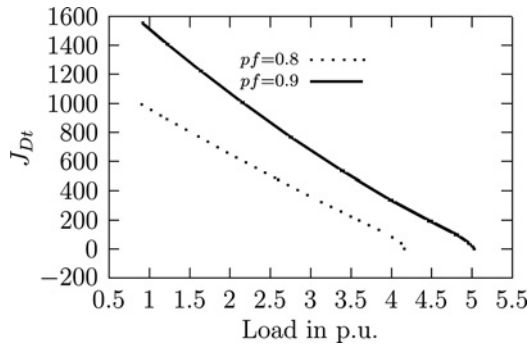


Fig. 6 $J_{Dt} - P_{Dk}$ curve for bus number 88 bus of IEEE 118 bus system, with load power factors $pf = 0.8$ and $pf = 0.9$

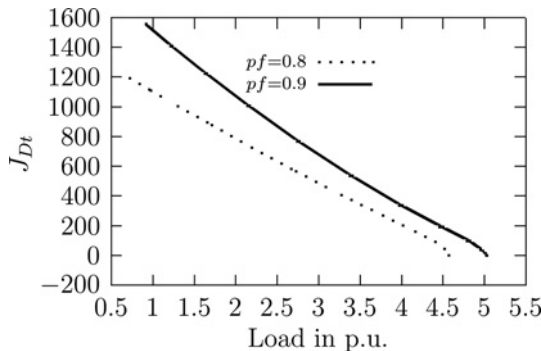


Fig. 7 $J_{Dt} - P_{Dk}$ curve for bus number 45 bus of IEEE 118 bus system, with load power factors $pf = 0.8$ and $pf = 0.9$

value for a bus reflects the voltage stability characteristic of the bus.

To examine the validity of the proposed measurement-based voltage stability analysis method, the voltage stability index VSI_k [14] and $ENVCI_k$ [16] are computed using the two consecutive load flow results, which is considered as time reference t_1 and t_2 during the simulation steps. Using the load flow results, the index VSI_k is represented as

$$VSI_k = 1 - \frac{|\hat{V}_k(t_2) - \hat{V}_k(t_1)\hat{I}_k(t_2)|}{|\hat{I}_k(t_2) - \hat{I}_k(t_1)\hat{V}_k(t_2)|} \quad (41)$$

where $\hat{V}_k(t_2)$, $\hat{V}_k(t_1)\hat{I}_k(t_1)$ and $\hat{I}_k(t_2)$ are the phasor bus voltages and bus current of the k th bus for time sample t_1 and t_2 .

The index $ENVCI_k$ is represented as:

$$ENVCI_k = 2(e_k(t_2)e_s - f_k(t_2)f_s) - (e_s^2 + f_s^2) \quad (42)$$

where $\hat{V}_k(t_2)$ ($V_k(t_2)\angle\delta_k = e_k(t_2) + jf_k(t_2)$) and \hat{E}_s ($E_s\angle\delta_s = e_s + jf_s$) are the node voltage of the target bus k and source voltage of the ESM, respectively. The ESM is derived using an ELNM proposed in the paper in [16]. The equivalent voltage of the ELNM is represented as

$$\hat{V}_{eq} = V_{eq}\angle\delta_{eq} = \frac{\sum_{i=1}^M \hat{V}_i y_{ki}}{\sum_{i=1}^M y_{ki}} \quad (43)$$

where M represents the number of transmission lines connected to the k th bus from the other buses of the system and y_{ki} represents the admittance of the transmission line connected from the i th bus of the system to the k th bus.

Taking \hat{V}_{eq} as the reference vector, the source voltage of the ESM is represented as

$$\hat{E}_s = KV_e'q + (1 - K)\hat{V}_k' \quad (44)$$

where $V_e'q = V_{eq}\angle 0$, $\hat{V}_k' = V_k\angle(\delta_k - \delta_{eq})$ and $\hat{E}_s' = E_s\angle\delta_s' = E_s\angle(\delta_s - \delta_{eq})$, respectively.

Using the two consecutive load flow results (which are considered as time reference t_1 and t_2 during the simulation steps), (44) can be represented as

$$\hat{E}_s' = KV_e'q(t_1) + (1 - K)\hat{V}_k'(t_1) \quad (45)$$

$$\hat{E}_s' = KV_e'q(t_2) + (1 - K)\hat{V}_k'(t_2) \quad (46)$$

Solving, (45) and (46) the factor K can be expressed as

$$K = \frac{1}{1 - ((V_e'q(t_1) - V_e'q(t_2))/\hat{V}_k'(t_1) - \hat{V}_k'(t_2))} \quad (47)$$

Substituting K in (44), \hat{E}_s' is determined as

$$\hat{E}_s' = E_s\angle\delta_s' = KV_e'q(2) + (1 - K)\hat{V}_k'(2) \quad (48)$$

Therefore the source voltage for the ESM is determined as

$$\hat{E}_s = E_s\angle\delta_s = E_s\angle(\delta_s' + \delta_{eq}) = e_s + jf_s \quad (49)$$

Substituting this value in (42), the index $ENVCI_k$ is determined.

Tables 1–3 represent the simulation results for load buses – 29, 21 and 7 of the IEEE 30 bus system with load power factor 0.8. Tables 4–6 represent the simulation results for load buses – 118, 88 and 45 of the IEEE 118 bus system with load power factor 0.8.

It has been observed from the simulation results presented in the tables for IEEE 30 and IEEE 118 bus systems that the J_{Dt} , $ENVCI_k$ and VSI_k close to zero as the system approaches the proximity of voltage collapse. On the other hand, f_i increases sharply when the system approaches the proximity of voltage collapse and becomes significantly large at the proximity of voltage collapse. But, J_{Dt} , f_i , $ENVCI_k$ and VSI_k cannot provide the measure of critical load of a load bus corresponding to its operating point.

On the other hand, the proposed method can predict the critical load P_{Dkt}^{crit} of a bus corresponding to its operating point. It has been observed that $P_{Dkt}^{predict}$ for the buses of both

Table 1 Critical predicted load at target load bus 29 of IEEE 30 bus system

| P_{Dk} | VSI_k | $ENVCI_k$ | J_{Dt} | f_t | P_{Dk}^{predt} | P_{Dk}^{crt} for $n = 1$ | P_{Dk}^{crt} for $n = 1.5$ |
|----------|---------|-----------|----------|--------------|------------------|----------------------------|------------------------------|
| 0.0630 | 0.9521 | 0.9217 | 4.309 | 8.46 | 0.5725 | 0.2923 | 0.2349 |
| 0.0843 | 0.9325 | 0.8940 | 3.924 | 8.35 | 0.5544 | 0.3049 | 0.2489 |
| 0.1109 | 0.9047 | 0.8567 | 3.445 | 8.21 | 0.5305 | 0.3158 | 0.2627 |
| 0.1425 | 0.8650 | 0.8071 | 2.878 | 8.04 | 0.5003 | 0.3237 | 0.2752 |
| 0.1778 | 0.8083 | 0.7424 | 2.251 | 7.88 | 0.4635 | 0.3273 | 0.2854 |
| 0.2136 | 0.7277 | 0.6608 | 1.620 | 7.78 | 0.4218 | 0.3256 | 0.2922 |
| 0.2456 | 0.6153 | 0.5622 | 1.054 | 7.89 | 0.3792 | 0.3190 | 0.2956 |
| 0.2699 | 0.4682 | 0.4502 | 0.614 | 8.56 | 0.3417 | 0.3100 | 0.2962 |
| 0.2848 | 0.2995 | 0.3331 | 0.321 | 10.55 | 0.3153 | 0.3020 | 0.2957 |
| 0.2919 | 0.1445 | 0.2234 | 0.151 | 15.91 | 0.3014 | 0.2973 | 0.2953 |
| 0.2946 | 0.0473 | 0.1343 | 0.068 | 29.36 | 0.2969 | 0.2959 | 0.2954 |
| 0.2953 | -0.0000 | 0.0707 | 0.027 | 68.29 | 0.2957 | 0.2955 | 0.2954 |
| 0.2955 | -0.0111 | 0.0321 | 0.009 | 189.26 | 0.2955 | 0.2955 | 0.2955 |
| 0.2956 | -0.1121 | -0.1180 | 0.000 | 1 455 328.54 | 0.2955 | 0.2955 | 0.2955 |

Table 2 Critical predicted load at target load bus 21 of IEEE 30 bus system

| P_{Dk} | VSI_k | $ENVCI_k$ | J_{Dt} | f_t | P_{Dk}^{predt} | P_{Dk}^{crt} for $n = 1$ | P_{Dk}^{crt} for $n = 1.5$ |
|----------|---------|-----------|----------|-----------|------------------|----------------------------|------------------------------|
| 0.3224 | 0.9238 | 0.9134 | 81.915 | 37.37 | 2.5142 | 1.3289 | 1.0754 |
| 0.4292 | 0.8932 | 0.8811 | 72.908 | 36.72 | 2.4146 | 1.3796 | 1.1361 |
| 0.5601 | 0.8502 | 0.8372 | 61.961 | 35.91 | 2.2854 | 1.4188 | 1.1927 |
| 0.7116 | 0.7900 | 0.7787 | 49.446 | 35.01 | 2.1240 | 1.4401 | 1.2404 |
| 0.8732 | 0.7063 | 0.7025 | 36.311 | 34.21 | 1.9345 | 1.4378 | 1.2742 |
| 1.0266 | 0.5920 | 0.6066 | 24.001 | 34.07 | 1.7310 | 1.4109 | 1.2915 |
| 1.1504 | 0.4440 | 0.4918 | 13.988 | 35.88 | 1.5402 | 1.3670 | 1.2942 |
| 1.2301 | 0.2717 | 0.3642 | 7.052 | 43.01 | 1.3941 | 1.3222 | 1.2830 |
| 1.2677 | 0.1075 | 0.2366 | 2.995 | 66.29 | 1.3129 | 1.2932 | 1.2826 |
| 1.2791 | -0.0017 | 0.1270 | 1.012 | 152.54 | 1.2857 | 1.2828 | 1.2814 |
| 1.2810 | -0.0354 | 0.0519 | 0.245 | 581.95 | 1.2814 | 1.2812 | 1.2811 |
| 1.2811 | -0.0064 | -0.0061 | 0.006 | 24 720.84 | 1.2811 | 1.2811 | 1.2811 |

Table 3 Critical predicted load at target load bus 7 of IEEE 30 bus system

| P_{Dk} | VSI_k | $ENVCI_k$ | J_{Dt} | f_t | P_{Dk}^{predt} | P_{Dk}^{crt} for $n = 1$ | P_{Dk}^{crt} for $n = 1.5$ |
|----------|---------|-----------|----------|-----------|------------------|----------------------------|------------------------------|
| 0.6138 | 0.9293 | 0.9256 | 509.664 | 91.28 | 6.1976 | 3.0923 | 2.4728 |
| 0.8273 | 0.9011 | 0.9002 | 466.665 | 90.05 | 6.0097 | 3.2290 | 2.6223 |
| 1.0982 | 0.8618 | 0.8653 | 412.380 | 88.46 | 5.7600 | 3.3493 | 2.7698 |
| 1.4276 | 0.8073 | 0.8180 | 346.959 | 86.53 | 5.4373 | 3.4396 | 2.9059 |
| 1.8043 | 0.7323 | 0.7549 | 273.182 | 84.47 | 5.0385 | 3.4845 | 3.0189 |
| 2.1989 | 0.6312 | 0.6728 | 197.242 | 82.92 | 4.5777 | 3.4720 | 3.0979 |
| 2.5644 | 0.5005 | 0.5700 | 127.836 | 83.49 | 4.0955 | 3.4035 | 3.1384 |
| 2.8497 | 0.3441 | 0.4485 | 72.794 | 90.04 | 3.6581 | 3.3002 | 3.1462 |
| 3.0244 | 0.1795 | 0.3163 | 35.415 | 113.26 | 3.3371 | 3.2004 | 3.1361 |
| 3.0989 | 0.0383 | 0.1884 | 13.828 | 194.30 | 3.1700 | 3.1391 | 3.1238 |
| 3.1160 | -0.0433 | 0.0843 | 3.615 | 598.64 | 3.1220 | 3.1194 | 3.1181 |
| 3.1168 | -0.0526 | 0.0188 | 0.270 | 7751.94 | 3.1168 | 3.1168 | 3.1168 |
| 3.1169 | -0.0170 | -0.0012 | 0.022 | 98 148.16 | 3.1168 | 3.1168 | 3.1168 |

the IEEE 30 and 118 bus system are considerably higher compared with that of the actual critical load (i.e. load at the point of collapse) of the buses, when the prediction is made under the condition when the system is far from the point of collapse. But, as the system approaches the proximity of voltage collapse, it goes close to the actual critical load of the bus. The normalised predicted critical load P_{Dk}^{crt} with $n = 1$ shows a slightly higher value when perdition is caused with the bus load which is far from the proximity of voltage collapse. Whereas, the normalised predicted critical load P_{Dk}^{crt} with $n = 1.5$ shows a slightly

lower value when perdition is caused with the bus load which is far from the proximity of voltage collapse. However, near the proximity of voltage collapse, they show the same value and are very close to the load where the system collapse would take place. Based on his practical experience about the system, a power system operator may select a suitable value of n for accurate prediction of critical load of a bus.

To illustrate these facts, a few simulation results for IEEE 30 and IEEE 118 bus systems are selected with the index $ENVCI_k$ value around 0.7 to examine the predicted load

Table 4 Critical predicted load at target load bus 118 of IEEE 118 bus system

| P_{Dk} | VSI_k | $ENVCI_k$ | J_{Dt} | f_t | P_{Dk}^{predt} | P_{Dk}^{crt} for $n = 1$ | P_{Dk}^{crt} for $n = 1.5$ |
|----------|---------|-----------|----------|---------------|------------------|----------------------------|------------------------------|
| 0.6090 | 0.9461 | 0.8713 | 355.836 | 78.34 | 5.1514 | 2.6729 | 2.1545 |
| 0.8121 | 0.9240 | 0.8431 | 320.778 | 77.15 | 4.9699 | 2.7816 | 2.2797 |
| 1.0630 | 0.8927 | 0.8051 | 277.723 | 75.67 | 4.7334 | 2.8711 | 2.3992 |
| 1.3573 | 0.8480 | 0.7546 | 227.649 | 73.96 | 4.4355 | 2.9292 | 2.5040 |
| 1.6781 | 0.7842 | 0.6891 | 173.647 | 72.30 | 4.0797 | 2.9439 | 2.5842 |
| 1.9940 | 0.6939 | 0.6068 | 121.004 | 71.48 | 3.6867 | 2.9100 | 2.6327 |
| 2.2649 | 0.5700 | 0.5084 | 75.877 | 73.26 | 3.3006 | 2.8367 | 2.6504 |
| 2.4591 | 0.4134 | 0.3983 | 42.555 | 81.59 | 2.9806 | 2.7508 | 2.6487 |
| 2.5702 | 0.2451 | 0.2863 | 21.481 | 105.74 | 2.7734 | 2.6847 | 2.6424 |
| 2.6194 | 0.1062 | 0.1855 | 9.902 | 169.46 | 2.6778 | 2.6524 | 2.6399 |
| 2.6360 | 0.0261 | 0.1073 | 4.248 | 336.44 | 2.6486 | 2.6432 | 2.6404 |
| 2.6405 | -0.0030 | 0.0560 | 1.744 | 770.95 | 2.6427 | 2.6417 | 2.6412 |
| 2.6414 | -0.0071 | 0.0271 | 0.707 | 1868.42 | 2.6418 | 2.6417 | 2.6416 |
| 2.6417 | -0.0016 | 0.0055 | 0.182 | 7261.45 | 2.6417 | 2.6417 | 2.6417 |
| 2.6418 | -0.0003 | 0.0013 | 0.143 | 9306.51 | 2.6418 | 2.6418 | 2.6418 |
| 2.6419 | 0.0766 | -0.0160 | -0.001 | -1 665 691.60 | 2.6418 | 2.6418 | 2.6418 |

Table 5 Critical predicted load at target load bus 88 of IEEE 118 bus system

| P_{Dk} | VSI_k | $ENVCI_k$ | J_{Dt} | f_t | P_{Dk}^{predt} | P_{Dk}^{crt} for $n = 1$ | P_{Dk}^{crt} for $n = 1.5$ |
|----------|---------|-----------|----------|-----------|------------------|----------------------------|------------------------------|
| 0.8975 | 0.8845 | 0.9166 | 989.795 | 127.87 | 8.6381 | 4.3552 | 3.4900 |
| 1.2079 | 0.8397 | 0.8897 | 891.721 | 125.41 | 8.3181 | 4.5257 | 3.6855 |
| 1.5990 | 0.7787 | 0.8524 | 769.779 | 122.25 | 7.8958 | 4.6622 | 3.8698 |
| 2.0681 | 0.6972 | 0.8012 | 626.721 | 118.46 | 7.3589 | 4.7439 | 4.0282 |
| 2.5927 | 0.5922 | 0.7323 | 472.235 | 114.54 | 6.7155 | 4.7516 | 4.1454 |
| 3.1234 | 0.4650 | 0.6421 | 322.811 | 111.91 | 6.0081 | 4.6788 | 4.2128 |
| 3.5910 | 0.3241 | 0.5288 | 196.253 | 113.73 | 5.3166 | 4.5425 | 4.2342 |
| 3.9299 | 0.1832 | 0.3954 | 103.060 | 127.75 | 4.7366 | 4.3813 | 4.2229 |
| 4.1098 | 0.0529 | 0.2509 | 43.143 | 181.92 | 4.3469 | 4.2435 | 4.1616 |
| 4.1516 | -0.0129 | 0.0579 | 5.423 | 938.09 | 4.1574 | 4.1549 | 4.1536 |
| 4.1534 | -0.0197 | 0.0243 | 1.532 | 3202.10 | 4.1539 | 4.1537 | 4.1536 |
| 4.1537 | -0.0083 | -0.0016 | 0.052 | 96 149.54 | 4.1537 | 4.1537 | 4.1537 |

Table 6 Critical predicted load at target load bus 45 of IEEE 118 bus system

| P_{Dk} | VSI_k | $ENVCI_k$ | J_{Dt} | f_t | P_{Dk}^{predt} | P_{Dk}^{crt} for $n = 1$ | P_{Dk}^{crt} for $n = 1.5$ |
|----------|---------|-----------|----------|-------------|------------------|----------------------------|------------------------------|
| 0.7154 | 0.8997 | 0.9154 | 1190.550 | 138.06 | 9.3389 | 4.4140 | 3.4929 |
| 0.9692 | 0.8607 | 0.8964 | 1108.464 | 136.31 | 9.1014 | 4.6136 | 3.7011 |
| 1.2961 | 0.8076 | 0.8704 | 1003.499 | 134.00 | 8.7847 | 4.7976 | 3.9102 |
| 1.7031 | 0.7364 | 0.8350 | 874.534 | 131.11 | 8.3734 | 4.9498 | 4.1097 |
| 2.1861 | 0.6440 | 0.7878 | 724.750 | 127.75 | 7.8594 | 5.0519 | 4.2864 |
| 2.7226 | 0.5301 | 0.7261 | 563.531 | 124.39 | 7.2529 | 5.0879 | 4.4271 |
| 3.2690 | 0.4011 | 0.6477 | 405.919 | 122.20 | 6.5907 | 5.0522 | 4.5241 |
| 3.7659 | 0.2704 | 0.5523 | 268.029 | 123.48 | 5.9365 | 4.9568 | 4.5789 |
| 4.1569 | 0.1536 | 0.4418 | 160.331 | 132.82 | 5.3641 | 4.8294 | 4.6001 |
| 4.4103 | 0.0593 | 0.3222 | 84.627 | 161.68 | 4.9337 | 4.7046 | 4.5878 |
| 4.5322 | -0.0118 | 0.2029 | 36.576 | 252.27 | 4.6771 | 4.6140 | 4.5831 |
| 4.5648 | -0.0572 | 0.0966 | 10.167 | 692.93 | 4.5794 | 4.5731 | 4.5699 |
| 4.5649 | -0.0737 | 0.0091 | 0.044 | 1 51 368.95 | 4.5649 | 4.5649 | 4.5649 |
| 4.5650 | 0.0011 | 0.0021 | -0.545 | -12 157.63 | 4.5650 | 4.5650 | 4.5650 |

margin and actual load margin of a bus. The predicted load margin and actual load margin of a bus are determined as

$$\Delta P_{Dk}^{crt} = P_{Dk}^{crt} - P_{Dk} \quad (50)$$

$$\Delta P_{Dk}^{PAVC} = P_{Dk}^{PAVC} - P_{Dk} \quad (51)$$

where P_{Dk}^{crt} , P_{Dk}^{PAVC} and P_{Dk} are predicted critical load of k th bus, actual critical load of the k th bus (i.e. load at k th bus at the point of actual voltage collapse (PAVC)) and P_{Dk} is the load at the k th bus, respectively, with $n = 1.5$.

The simulation results indicate that corresponding to $ENVCI_{29} = 0.6608$, $ENVCI_{21} = 0.7025$, $ENVCI_7 = 0.6728$ for 29, 21 and 7 buses of the IEEE 30 system, the predicted

and actual load margin of the buses are as follows

$$\Delta P_{D29}^{\text{crt}} = 0.2922 - 0.2136 = 0.0786 \text{ pu;}$$

$$\Delta P_{D29}^{\text{PAVC}} = 0.2956 - 0.2136 = 0.0820 \text{ pu}$$

$$\Delta P_{D21}^{\text{crt}} = 1.2742 - 0.8732 = 0.4010 \text{ pu;}$$

$$\Delta P_{D21}^{\text{PAVC}} = 1.2811 - 0.8732 = 0.4079 \text{ pu}$$

$$\Delta P_{D7}^{\text{crt}} = 3.0979 - 2.1989 = 0.8990 \text{ pu;}$$

$$\Delta P_{D7}^{\text{PAVC}} = 3.1169 - 2.1989 = 0.9180 \text{ pu}$$

Similarly, the simulation results indicate that corresponding to $\text{ENVCI}_{118} = 0.6068$, $\text{ENVCI}_{88} = 0.7323$ and $\text{ENVCI}_{45} = 0.6477$ for 118, 88 and 45 buses of IEEE 118 system, the predicted and actual load margin of the buses are as follows

$$\Delta P_{D118}^{\text{crt}} = 2.6327 - 1.9940 = 0.6387 \text{ pu;}$$

$$\Delta P_{D118}^{\text{PAVC}} = 2.6419 - 1.9940 = 0.6479 \text{ pu}$$

$$\Delta P_{D88}^{\text{crt}} = 4.1454 - 2.5927 = 1.5527 \text{ pu;}$$

$$\Delta P_{D88}^{\text{PAVC}} = 4.1537 - 2.5927 = 1.561 \text{ pu}$$

$$\Delta P_{D45}^{\text{crt}} = 4.5241 - 3.2690 = 1.2551 \text{ pu;}$$

$$\Delta P_{D45}^{\text{PAVC}} = 4.5650 - 3.2690 = 1.2960 \text{ pu}$$

The analysis shows that at a similar value of the index ENVCI_k , the load margin may be different for different buses of a system. In addition to this, the load margin of the load buses of the IEEE 118 bus system with a similar value of the index ENVCI_k is more than the load margin of the load buses of the IEEE 30 bus system. Therefore the ENVCI_k could not provide information/measure about the load margin of a load bus. On the other hand, the load margin predicted by the proposed method offers a good measure of load margin of a bus with respect to its PAVC. This measure would be important information for a power system operator while managing a system operation under the heavily loaded condition of a power system.

The simulations were carried out in a PC with Pentium-4 processor having a processor speed of 1.5 GHz and the LINUX operating system. The CPU time required to implement the computational steps described in Section 6 is less than 0.1 μs (because the computational steps require processing of a two by two matrix only). Therefore it can be implemented for real-time monitoring of the voltage stability of a power system.

8 Conclusion

A new method is proposed for monitoring the voltage stability of a power system based on two consecutive measurements of real power, reactive power and voltage of a bus. The bus measurements are used to determine the elements of the Jacobian matrix of a TBES with respect to a target bus. Furthermore, a sensitivity relation between the change in the determinant of the Jacobian matrix of the TBES with respect to a change in real-power injection at the target bus has been developed using the elements of the Jacobian matrix of the TBES and its bus voltage magnitude. This relation is then used to predict the critical load of the bus with respect to its voltage stability limit.

The advantage of this voltage stability monitoring process is that it is independent of power system modelling and thus does not suffer from inaccuracy owing to uncertainty in modelling parameters. The simulation results for the IEEE 30 and the IEEE 118 bus systems demonstrate the validity and applicability of the method.

9 References

- 1 IEEE/CIGRE, Joint Task Force on Stability Terms and Definitions: 'Definition and classification of power system stability', *IEEE Trans. Power Syst.*, 2004, **19**, (3), pp. 1387–1401
- 2 Clark, H.K.: 'New challenges: voltage stability', *IEEE Power Eng. Rev.*, 1990, **10**, (4), pp. 33–37
- 3 Kessel, P., Glavitsch, H.: 'Estimating the voltage stability of a power system', *IEEE Trans. Power Deliv.*, 1986, **PWRD-1**, (3), pp. 346–354
- 4 Gubina, F., Strmcnk, B.: 'Voltage collapse proximity index determination using voltage phaser approach', *IEEE Trans. Power Syst.*, 1995, **10**, (2), pp. 788–793
- 5 Sinha, A.K., Hazarika, D.: 'Comparative study of voltage stability indices in a power system', *Int. J. Electr. Power Energy Syst.*, 2000, **22**, (8), pp. 589–596
- 6 Tamura, Y., Mori, H., Lwanoto, S.: 'Relationship between voltage instability and multiple load flow solutions in electrical system', *IEEE Trans.*, 1983, **PAS-102**, pp. 115–1125
- 7 Crisan, O., Liu, M.: 'Voltage collapse prediction using an improved sensitivity approach', *Electr. Syst. Res.*, 1994, **28**, pp. 181–190
- 8 Lof, P.A., Anderson, G., Hill, D.J.: 'Voltage stability indices of stressed power system', *IEEE Trans. PWRD*, 1993, **8**, (1), pp. 326–335
- 9 Tiranuchit, A., Thomas, R.J.: 'A posturing strategy against voltage instability in electrical power systems', *IEEE Trans. PWRD*, 1989, **3**, (1), pp. 87–93
- 10 Ajarapu, V., Christy, C.: 'The continuation power flow – a tool for steady state voltage stability analysis', *IEEE Trans. Power Syst.*, 1992, **7**, (1), pp. 416–423
- 11 Souza, A.C., Quintana, V.H.: 'New technique of network partitioning for voltage collapse margin calculation', *IEE Proc. Gener. Transm. Distrib.*, 1994, **141**, (6), pp. 630–636
- 12 Vu, K., Begovic, M.M., Novosel, D., Saha, M.M.: 'Use of local measurements to estimate voltage stability margin', *IEEE Trans. Power Syst.*, 1999, **14**, (3), pp. 1029–1035
- 13 Haque, M.H.: 'On-line monitoring of maximum permissible loading of a power system within voltage stability limits', *IEE Proc. Gener. Transm. Distrib.*, 2003, **150**, (1), pp. 109–112
- 14 Smon, I., Verbic, G., Gubina, F.: 'Local voltage-stability index using Tellegen's theorem', *IEEE Trans. Power Syst.*, 2006, **21**, (3), pp. 1267–1275
- 15 Sandro, C., Taranto, G.N.: 'A real-time voltage instability identification algorithm based on local phasor measurements', *IEEE Trans. Power Syst.*, 2008, **23**, (3), pp. 1271–1279
- 16 Wang, Y., Li, W., Lu, J.: 'A new node voltage stability index based on local voltage phasors', *Electr. Power Syst. Res.*, 2009, **79**, pp. 265–271
- 17 Glavic, M., Cutsem, T.V.: 'Wide-area detection of voltage instability from synchronized phsor measurements. Part I: principle', *IEEE Trans. Power Syst.*, 2009, **24**, (3), pp. 1408–1416
- 18 Glavic, M., Cutsem, T.V.: 'Wide-area detection of voltage instability from synchronized phsor measurements. Part II: simulation results', *IEEE Trans. Power Syst.*, 2009, **24**, (3), pp. 1417–1425
- 19 Diao, R., Sun, K., Vittal, V., *et al.*: 'Decision Treebased online voltage security assessment using PMU measurements', *IEEE Trans. Power Syst.*, 2009, **24**, (2), pp. 832–839
- 20 Musirin, I., Rahman, T.K.A.: 'On-line voltage stability based contingency ranking using fast voltage stability index', *Proc. IEEE/PSE*, 2002, 2002, **2**, pp. 1118–1123
- 21 Juan, Y., Wenyuan, L., Wei, Y.: 'Querying effectiveness of several existing line-based voltage stability indices', *Proc. CSEE*, 2009, **29**, (19), pp. 27–35
- 22 Fu, L., Pal, B.C., Cory, J.: 'Phasor measurement application for power system voltage stability monitoring'. General Meeting of the IEEE Power and Energy Society, IEEE 2008, pp. 4953–4960
- 23 Phadke, A.R., Fozdar, M., Niazi, K.R.: 'A new technique for on-line monitoring of voltage stability margin using local signals'. 15th National Power Systems Conf. (NPSC), Bombay, December 2008, IIT, pp. 488–492